Fabrication and Characterization of Single-Crystalline ZnTe Nanowire Arrays

Liang Li, Youwen Yang, Xiaohu Huang, Guanghai Li,* and Lide Zhang

Key Laboratory of Materials Physics, Institute of Solid State Physics, Chinese Academy of Sciences, Hefei 230031, People's Republic of China

Received: March 8, 2005; In Final Form: April 20, 2005

Semiconductor ZnTe nanowire arrays have been synthesized by the pulsed electrochemical deposition from aqueous solutions into porous anodic alumina membranes. X-ray diffraction analyses show that the as-synthesized nanowires have a highly preferential orientation. Scanning electron microscopy, transmission electron microscopy, and high-resolution transmission electron microscopy indicate that high-filling, ordered, and single-crystalline nanowire arrays have been obtained. The optical absorption spectra of the nanowire arrays show that the optical absorption band edge of the ZnTe nanowire array exhibits a blue shift compared with that of bulk ZnTe. The growth mechanism and the electrochemical deposition process are discussed together with the chemical compositions analysis.

Introduction

One-dimensional (1D) semiconductor nanostructures have received much attention due to their novel properties and potential applications in nanoscale electronics and optoelectronics.[1] Among these semiconductor systems, the II−VI family of the compound semiconductors, including ZnO, ZnSe, CdSe, and CdTe, has been widely studied because of their potential applications in solar cells, photodetectors, and light emitting diodes.[2−7] Many attempts have been made to fabricate 1D nanostructures, such as high-temperature chemical vapor deposition (CVD),[8,9] solvothermal route,[10] and template-assisted method.[11−14] Among these methods, the anodic alumina membrane (AAM)-based synthesis is a widely used route for fabricating 1D nanostructures, because the AAMs possess a uniform and parallel porous structure, which can be used as templates to assemble high-quality nanowire and nanotube arrays.[15−21]

Zinc telluride (ZnTe), one of the important semiconductor materials with a direct optical band gap of 2.2−2.3 eV at room temperature, has potential applications in optoelectronic and thermoelectric devices.[22] Various techniques have been reported for the fabrication of ZnTe thin films, such as thermal vacuum evaporation,[23] vapor-phase epitaxy,[24] molecular beam epitaxy,[25] and electrochemical deposition.[26−28] Because the Te^{2+} is difficult to dissolve and easy to precipitate, electrochemical deposition of compounds of Te^{2+} is very difficult in aqueous solution. To the best of our knowledge, there are no reports of the fabrication of the ZnTe nanowire arrays.

In this paper, large-scale, ordered, and single-crystalline ZnTe nanowire arrays have been fabricated in AAM using the pulsed electrochemical deposition technique from an aqueous solution for the first time.

Experimental Procedures

The AAM templates were prepared using a two-step anodization process as described previously.[29−32] The pore size of the AAM used was about 60 nm. A layer of Au film (thickness, 200 nm) was sputtered onto one side of the AAM to serve as the working electrode in a two-electrode plating cell, and a graphite plate was used as the counter electrode. The pulsed electrochemical deposition was carried out at a constant current density of 10 mA/cm^2 at 330 K. During the pulsed time, species were reduced on the pore ground. The delayed time provided time for the recovery of the ion concentration.[33−35] Here both the pulsed time and delayed time were 100 ms. The electrolyte was prepared by dissolving 10 mM $ZnSO_4$, 0.15 mM TeO_2, 0.2 M $C_6H_8O_7{\cdot}H_2O$ ($H_3Cit.H_2O$), and 0.2 M $Na_3C_6H_5O_7{\cdot}2H_2O$ ($Na_3Cit{\cdot}2H_2O$) in water. Due to the low solubility of TeO_2 continuous heating and stirring for several hours is required. The pH of the final electrolyte was adjusted to 3.5 with H_2SO_4.

Power X-ray diffraction (XRD, D/MAX-rA), field-emission scanning electron microscopy (FE-SEM, JEOL JSM-6700F), transmission electron microscopy (TEM, H-800), selected area electron diffraction (SAED), and high-resolution transmission electron microscopy (HRTEM, JEOL-2010) were used to study the crystalline structure and morphology of nanowire arrays. The chemical compositions of the nanowires were determined by energy dispersive spectrometer (EDS). The band structure of the nanowires was obtained by measuring the optical absorption spectra on UV−visible spectrophotometer (Cary-5E). For XRD and optical absorption measurements, the overfilled nanowires on the surface of the AAM and the back Au film were mechanically polished away using Al_2O_3 nanopowders. For SEM observation, the AAM was partly dissolved with 0.5 M NaOH solution and then carefully rinsed with deionized water several times. For TEM and HRTEM observations, the AAM was completely dissolved with 1 M NaOH solution and then rinsed with absolute ethanol.

Results and Discussion

Figure 1 shows the XRD pattern of the as-prepared ZnTe nanowire array. All the peaks can be indexed to the cubic ZnTe structure (JCPDS No. 75-2085). The intensity of the (220) diffraction is much higher than all the other peaks, indicating that the ZnTe nanowires have a preferential orientation along the [220] direction, which will be further conformed by HRTEM

* Corresponding author. Fax: +86-551-5591434. E-mail address: ghli@issp.ac.cn.

10.1021/jp0511855 CCC: $30.25
Published on Web 06/07/2005

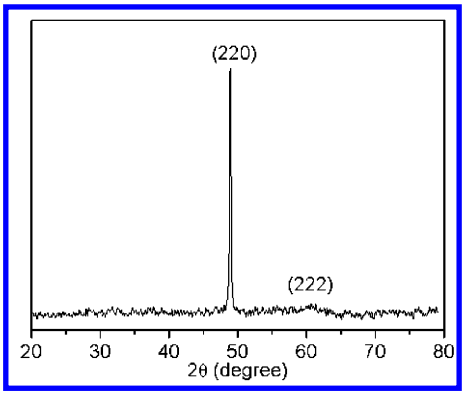

Figure 1. XRD pattern of ZnTe nanowire array.

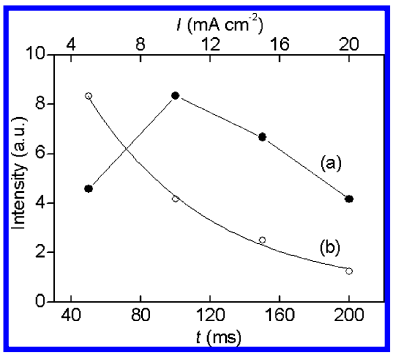

Figure 2. Relative intensity of the (220) peak of ZnTe nanowires as a function of (a) current density (*I*) and (b) pulsed time (*t*), keeping the delayed time at 100 ms.

analysis. In addition, no diffraction peaks from the elemental Zn and Te can be detected.

Figure 2 shows the dependence of the (220) peak intensity of XRD patterns of the ZnTe nanowires on the current density and pulsed time. One can see that the peak intensity first increases, after reaching a maximum value at the current density of 10 mA/cm^2, and then decreases with further increasing of the current density. The reduction in the peak intensity might be due to the hydrogen evolution at larger current densities, which suppresses the growth of the nanowires along the (220) orientation. Keeping the delayed time at constant 100 ms, the (220) peak intensity always decreases with increasing pulsed time. This result indicates that the best crystallinity of the ZnTe nanowires can be obtained at the current density of about 10 mA/cm^2 and the pulsed time of about 100 ms.

Figure 3 shows SEM images of the as-prepared AAM and the ZnTe nanowire array. Figure 3a is a typical image of the as-prepared empty AAM. One can see that the AAM has a highly ordered pore array with an average pore size of about 60 nm. The morphologies of the ZnTe nanowire arrays after different etching times are represented in Figure 3b−d. Parts b and c of Figure 3 are the surface images of the nanowire arrays after etching for 3 and 10 min, respectively. Apparently, the nanowires are high filling (nearly 100%) and the exposed parts of the nanowires increase with increasing etching time. Figure 3d shows the cross-sectional image of the ZnTe nanowire array with a length as long as about 45 μm after etching for 15 min. The length of the nanowires is the same as the thickness of the AAM used, because the deposition of the nanowires starts at the Au cathode on the bottom of the pores, and then the nanowires grow along the pores until the top of the AAM. It is noted that all the ZnTe nanowires have the same length, implying that the electrodeposition process is well-controlled and all the nanowires grow along the pores at the same rate.

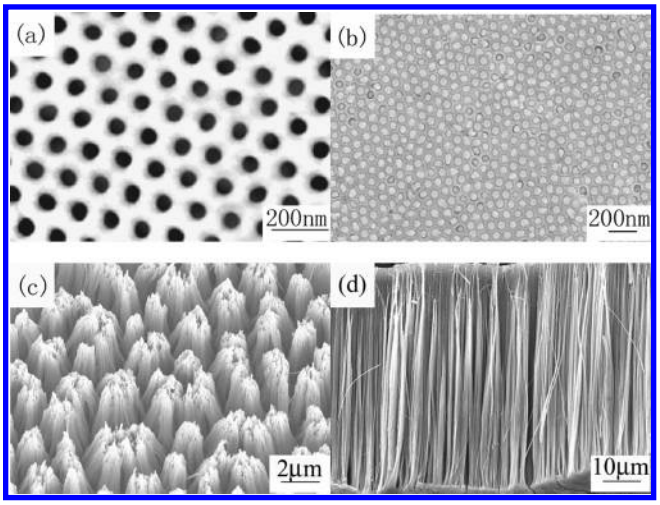

Figure 3. SEM images of empty AAM (a) and ZnTe nanowire arrays: (b and c) top views of the ZnTe nanowire array after etching for 3 and 10 min, respectively; (d) cross-sectional view of ZnTe nanowire array after etching for 15 min.

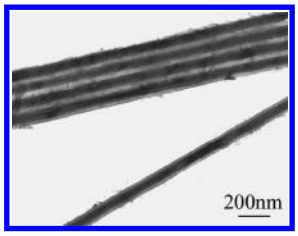

Figure 4. TEM image of the ZnTe nanowire array.

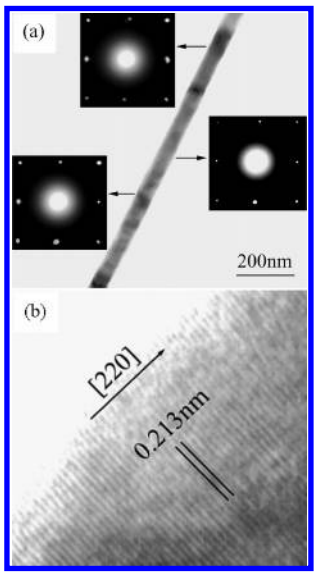

Figure 5. (a) TEM image of a single ZnTe nanowire and its SAED patterns along the nanowire length. (b) HRTEM image of the nanowire in a.

Figure 4 shows a typical TEM image of the ZnTe nanowires. It is evident that the ZnTe nanowires with a smooth surface and a high aspect ratio still inside the nanochannels of AAM can be clearly seen. The diameters of the nanowires are uniform and equal to the pore size of the AAM used.

Figure 5 shows the SAED patterns and HRTEM image of a segment of a randomly selected ZnTe nanowire. One can see that the nanowire is dense and uniform in diameter corresponding to the pore size of the AAM. It is noticed that there are some contrast variations along the nanowires. The SAED patterns taken along the nanowire (Figure 5a) do not change

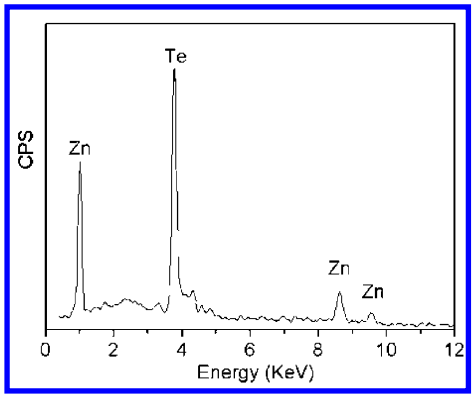

Figure 6. EDS spectrum of the ZnTe nanowire array.

TABLE 1: Atomic Percentages of ZnTe Nanowires as a Function of Zn Concentration in the Solution

Zn concn (mM)	Te concn (mM)	Zn:Te
20	0.15	52:48
15	0.15	51:49
10	0.15	50:50
5	0.15	49:51

except for a slight variation in the intensity of the individual spots, which indicates that the nanowire is single-crystalline. The variation in the intensity of the individual spots might come from slightly structural deformation along the length in the release process of the nanowires from the membrane. The same phenomena were also observed in other nanosystems, such as nanowire, nanobelt, and nanosheet.[18,36−38] The lattice-resolved image of the nanowire further reveals that the nanowire is structural uniform and single-crystalline, with an interplanar spacing corresponding to the (220) plane of cubic ZnTe (Figure 5b). This result indicates that the growth direction of ZnTe nanowire is along the [220] direction, which is in agreement with the XRD result.

The EDS spectrum of ZnTe nanowires is shown in Figure 6, which proves that the nanowires consist of only Zn and Te. The quantitative analysis of the EDS spectrum indicates that the atomic ratio of Zn to Te is close to 1:1. It is well-known that a high Zn^{2+} concentration in the electrolyte is necessary for the deposition of ZnTe thin films in order to bring the electrode potentials of the Zn^{2+} closer to Te^{2+}. To confirm the feasibility for nanowire growth, the electrolytes with different Zn^{2+} concentrations were used to grow ZnTe nanowires. The resulting EDS analyses are shown in Table 1. From this table one can see that the compositions of the nanowires are stoichiometric in despite of a wide range of the Zn^{2+} concentration in the electrolytes, which indicates that we can use a high Zn^{2+} concentration in the electrolyte to co-deposit a ZnTe nanowire array. It is worthy to note that the potential has a very important influence on the compositions of ZnTe nanowires. It was found that the ZnTe nanowires deposited at about −2.0 V exhibited a stoichiometric composition with Zn/Te ratio of 50:50, and that deposited at more negative potentials (<−2.3 V) exhibited a Zn-rich phase, while that deposited at more positive potentials (>−1.6 V) revealed a Te-rich phase.

Figure 7 shows the optical absorption spectra of the blank AAM and the ZnTe nanowires/AAM assembly system with the diameter of 60 nm (Figure 7a) and 40 nm (Figure 7b). It can be seen that the absorption spectrum of the ZnTe nanowires/AAM assembly system is quite different from that of the blank AAM, which is due to the absorption of ZnTe nanowires. It is known that the relationship between the absorption coefficient (α) near the absorption edge and the optical band gap (E_g) for direct interband transitions obeys the following formula:[39]

$$(\alpha h\nu)^2 = A(h\nu - E_g) \quad (1)$$

where A is the parameter that related to the effective masses associated with the valence and conduction bands, and $h\nu$ is the photon energy. Hence, the optical band gap for the absorption edge can be obtained by extrapolating the linear portion of the plot $(\alpha h\nu)^2$ versus $\alpha = 0$. The two insets (top-right corner in Figure 7a,b) show the $(\alpha h\nu)^2$ versus $h\nu$ plots for the two samples. For all samples, the optical absorption in the edge region can be well-fitted by the relation $(\alpha h\nu)^2 \propto h\nu - E_g$, which shows that the ZnTe nanowires embedded in the AAM have a direct band gap. The band gap of nanowires with diameters of 60 and 40 nm is about 3.43 and 3.52 eV, respectively. The shift of 40 nm nanowires is higher than that of 60 nm nanowires. This result indicates that the optical band edge of the ZnTe nanowires embedded in AAM exhibits a marked blue shift with respect to that of the bulk and thin-film ZnTe (2.2−2.3 eV).[23−28] The blue shift could be attributed to the quantum size effect, which has also been observed in other semiconductor nanosystems.[40−42]

The exciton Bohr radius (α_B) plays an important role in quantum confinement effect. If $R/\alpha_B < 4$ (R is the radius of particle), the quantum confinement is very obvious. The exciton Bohr radius can be estimated by the following formula: $\alpha_B = \epsilon h^2/4\pi^2\mu e^2$, where ϵ is the static dielectric constant, h is Planck's constant, μ is the reduced mass of an electron hole pair, $1/\mu = 1/m_e + 1/m_h$, m_e and m_h are the effective mass of electron and hole, respectively, and e is the electronic charge.[43] For ZnTe, $m_e = 0.09m_0$, $m_h = 0.6m_0$, $\epsilon = 10.1$;[44] thus α_B can be calculated to be about 6.2 nm. In the present study, R/α_B is smaller than 4 for 40 nm ZnTe nanowires and that is slightly larger than 4 for 60 nm nanowires. Therefore, ZnTe nanowires have a relative strong quantum confinement effect and exhibit a marked blue shift. The shift for 40 nm ZnTe nanowires is larger than that for 60 nm ZnTe nanowires.

Simple electrochemical calculation indicates that the formation of ZnTe alloy can be realized by using present experimental conditions. The basic electrochemical reactions for the simultaneous co-deposition of Zn and Te and their corresponding Nernst relations are as follows:

$$HTeO_2^+ + 3H^+ + 4e^- = Te + 2H_2O$$

$$E_{Te} = E_{Te}^{\ 0} - 0.0443\ pH + 0.0148 \log[HTeO_2^+]$$

$$E_{Te}^{\ 0} = 0.351\ V \quad (2)$$

$$Zn(Cit)_2^{\ 4-} + 4H^+ + 2e^- = Zn + 2H_2Cit^-$$

$$E_{Zn} = E_{Zn}^{\ 0} - 0.118pH - 0.0591 \log[H_2Cit^-] + 0.0295 \log[Zn(Cit)_2^{\ 4-}]$$

$$(2.98 < pH < 4.35)$$

$$E_{Zn}^{\ 0} = -0.542\ V \quad (3)$$

where, $E_{Zn}^{\ 0}$ and $E_{Te}^{\ 0}$ are the standard reduction potentials of Zn and Te (Ag/AgCl), respectively. E_{Zn} and E_{Te} are the equilibrium potentials of Zn and Te. E_{Zn} is calculated from the complex formation constant of Zn and citrate.[45]

It is known that underpotential deposition of the less noble constituent (in this case, Zn) of a compound (i.e. ZnTe) is brought by the gain of free energy caused by its formation. The

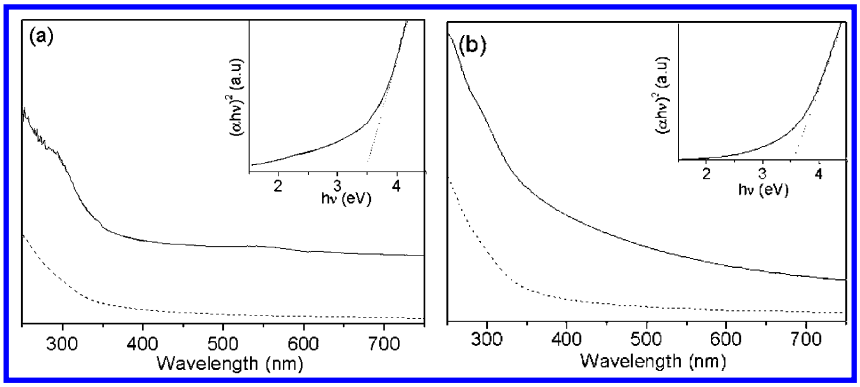

Figure 7. Optical absorption spectra of the empty AAM (dash lines) and ZnTe/AAM nanowire arrays (solid lines) with different diameters: (a) 60 and (b) 40 nm. The insets are the plots of $(\alpha h\nu)^2$ vs $h\nu$.

negative free energy, ΔG, occurring due to the formation of ZnTe leads to a positive shift in the deposition potential of Zn, ΔE, as given by[46]

$$\Delta G = -141.6 \text{ kJ mol}^{-1},\ \Delta E = -\frac{\Delta G}{nF} = 0.734 \text{ V} \quad (4)$$

In this case, a single-step deposition of the compound is possible between E_{Zn} and $E_{Zn} + |\Delta G/nF|$, and the stoichiometry should be independent of the concentration of Zn. Thus, it is expected to use a high concentration of Zn and a low concentration of Te to bring the electrode potentials of the two deposits closer.

To obtain a high-filling, uniform, and single-crystalline ZnTe nanowire array by the electrochemical deposition into the nanochannels of the AAM, several factors should be considered. First, before electrodeposition the AAM should be ultrasonicated in water for a few minutes to remove the impurities and air bubble inside the nanochannels, because the ZnTe ions will preferentially nucleate and grow at the sites of the impurities, causing the inhomogeneous growth of nanowires, and the air bubbles will hinder the ions to diffuse into the nanopores of the AAM, causing the electrodeposition on the surface of the AAM. Second, a suitable deposition rate is critical to obtain dense, ordered, and single-crystalline nanowires. To avoid the rapid nucleation and growth and inhomogeneous concentration gradient in the nanopores, the pulsed electrodeposition technique is employed, which allows a better control over the deposition parameters, such as deposition rate and ion concentration at the deposition interface, as compared with the direct and alternating current deposition.[47−50] In this paper, the pulsed time in each pulse cycle was so short (100 ms) that only a small number of metal ions at the interfaces are consumed. The delayed time (100 ms) provided enough time for the concentration of the metal ions at the pore tips to achieve steady state through diffusion. No evident concentration gradient near the reaction interface exists during the deposition, and the pulsed time controls the atom-by-atom deposition of nanowires, which improves the homogeneity of the deposition and makes the deposited nanowires have a highly preferential orientation and good crystallization. Proper choice of the pH value of the electrolyte and deposition potential is also important.

Conclusions

In summary, high-filling and ordered ZnTe nanowire arrays have been prepared from aqueous solutions by the pulsed electrochemical deposition into the pores of AAM. The ZnTe nanowires are single-crystalline and have a preferential orientation along the [110] direction. The optical absorption band edge of ZnTe nanowires exhibits a marked blue-shift compared with that of bulk ZnTe due to quantum size effect. We believe that the ZnTe nanowire arrays will find interesting applications in optoelectronic and thermoelectric nanodevices in the future.

Acknowledgment. This work was supported by the National Natural Science Foundation of China (Grant No. 10474098).

References and Notes

(1) Wang, Z. L. *Adv. Mater*. **2000**, *12*, 129.
(2) Liu, C. H.; Zapien,; J. A.; Yao, Y,; Meng, X. M.; Lee, C. S.; Fan, S. S.; Lifshitz, Y.; Lee, S. T. *Adv. Mater*. **2003**, *15*, 838.
(3) Service, R. F. *Science* **1997**, *276*, 895.
(4) Wang, Y. C.; Leu, I. C.; Hon, M. H. *J. Appl. Phys*. **2004**, *95*, 1444.
(5) Zhang, X. T.; Liu, Z.; Lp, K. M.; Leung, Y. P.; Li, Q.; HarK, S. K. *J. Appl. Phys*. **2004**, *95*, 5752.
(6) Xu, D. S.; Shi, X. S.; Guo, G. L.; Gui, L. L.; Tang, Y. Q. *J. Phys. Chem. B* **2000**, *104*, 5061.
(7) Yang, Q.; Tang, K. B.; Wang, C. R.; Qian, Y. T.; Zhang, S. Y. *J. Phys. Chem. B* **2002**, *106*, 9227.
(8) Chang, P. C.; Fan, Z. Y.; Wang, D. W.; Tseng, W. Y.; Chiou, W. A.; Hong, J.; Lu, J. G. *Chem. Mater*. **2004**, *16*, 5133.
(9) Malandrino, G.; Finocchiaro, S. T.; Nigro, R. L.; Bongiorno, C.; Spinella, C.; Fragalá, I. L. *Chem. Mater*. **2004**, *16*, 5559.
(10) Hu, H. M.; Yang, B. J.; Li, Q. W.; Liu, X. Y.; Yu, W. C.; Qian, Y. T. *J. Cryst. Growth* **2004**, *261*, 485.
(11) Jin, C. G.; Zhang, G. Q.; Qian, T.; Li, X. G.; Yao, Z. *J. Phys. Chem. B* **2004**, *108*, 1844.
(12) Choi, J.; Sauer, G.; Nielsch, K.; Wehrspohn, R. B.; Gösele, U. *Chem. Mater*. **2003**, *15*, 776.
(13) Guo, Y. G.; Wan, L. J.; Bai, C. L. *J. Phys. Chem. B* **2003**, *107*, 5441.
(14) Mukherjee, P. K.; Chakravorty, D. *J. Appl. Phys*. **2004**, *95*, 3164.
(15) Sander, M. S.; Gronsky, R.; Sands, T.; Stacy, A. M. *Chem. Mater*. **2003**, *15*, 335.
(16) Lakshmi, B. B.; Patrissi, C. J.; Martin, C. R. *Chem. Mater*. **1997**, *9*, 2544.
(17) Guo, Y. G.; Hu, J. S.; Liang, H. P.; Wan, L. J.; Bai, C. L. *Adv. Funct. Mater*. **2005**, *15*, 196.
(18) Miao, Z.; Xu, D. S.; Ouyang, J. H.; Guo, G. L.; Zhao, X. S.; Tang, Y. Q. *Nano Lett*. **2002**, *2*, 717.
(19) Martin-Gonzalez, M.; Prieto, A. L.; Gronsky, R.; Sands, T.; Stacy, A. M. *Adv. Mater*. **2003**, *15*, 1003.
(20) Zhang, Y.; Li, G. H.; Wu, Y. C.; Zhang, B.; Song, W. H.; Zhang, L. D. *Adv. Mater*. **2002**, *14*, 1227.
(21) Sander, M. S.; Cote, M. J.; Gu, W.; Kile, B. M.; Tripp, C. P. *Adv. Mater*. **2004**, *16*, 2052.
(22) Mingo, N. *Appl. Phys. Lett*. **2004**, *85*, 5986.
(23) Raju, K. U.; Vijayalakshmi, R. P.; Venugopal, R.; Reddy, D. R.; Reddy, B. K. *Mater. Lett*. **1992**, *13*, 336.
(24) Khan, M. R. H. *J. Phys. D: Appl. Phys*. **1994**, *27*, 2190.
(25) Tao, W. I.; Jurkovice, M.; Wang, I. W. *Appl. Phys. Lett*. **1994**, *64*, 1848.
(26) Chaure, N. B.; Jayakrishnan, R.; Nair, J. P.; Pandey, R. K. *Semicond. Sci. Technol*. **1997**, *12*, 1171.
(27) Lin, M. C.; Chen, P. Y.; Sun, I. W. *J. Electrochem. Soc*. **2001**, *148*, C653.
(28) Bozzini, B.; Baker, M. A.; Cavallotti, P. L.; Cerri, E.; Lenardi, C. *Thin Solid Films* **2000**, *361*, 388.
(29) Xu, D. S.; Xu, Y. J.; Chen, D. P.; Guo, G. L.; Gui, L. L.; Tang, Y. Q. *Adv. Mater*. **2000**, *12*, 520.

(30) Masuda, H.; Fukuda, K. *Science* **1995**, *268*, 1466.
(31) Xue, D. S.; Shi, H. G. *Nanotechnology* **2004**, *15*, 1752.
(32) Zhou, Y.; Li, H. L. *J. Mater. Chem.* **2002**, *37*, 5261.
(33) Nielsch, K.; Muller, F.; Li, A. P.; Gösele, U. *Adv. Mater.* **2000**, *12*, 582.
(34) Guo, Y. G.; Wan, L. J.; Zhu, C. F.; Yang, D. L.; Chen, D. M.; Bai, C. L. *Chem. Mater.* **2003** *15*, 664.
(35) Li, L.; Zhang, Y.; Li, G. H.; Zhang, L. D. *Chem. Phys. Lett*. **2003**, *378*, 244.
(36) Tian, M. L.; Wang, J. G.; Snyder, J.; Kurtz, J.; Liu, Y.; Schiffer, P.; Mallouk, T. E.; Chan, M. H. W. *Appl. Phys. Lett*. **2003**, *83*, 1620.
(37) Zhang, J.; Jiang, F. H.; Zhang, L. D. *J. Phys. Chem. B* **2004**, *108*, 7002.
(38) Dai, Z. R.; Pan, Z. W.; Wang, Z. L. *J. Phys. Chem. B* **2002**, *106*, 902.
(39) Peng, X. S.; Meng, G. W.; Zhang, J.; Zhao, L. X.; Wang, X. F.; Wang, Y. W.; Zhang, L. D. *J. Phys. D: Appl. Phys.* **2001**, *34*, 3224.
(40) Yu, D. B.; Yu, S. H.; Zhang, S. Y.; Zuo, J.; Wang, D. B.; Qian, Y. T. *Adv. Funct. Mater*. **2003**, *13*, 497.
(41) Gates, B.; Mayers, B.; Cattle, B.; Xia, Y. N. *Adv. Funct. Mater*. **2002**, *12*, 219.
(42) Park, W. I.; An, S. J.; Yang, J. L.; Yi, G. C.; Hong, S.; Joo, T.; Kim, M. *J. Phys. Chem. B* **2004**, *108*, 15457.
(43) Kayanuma, Y. *Phys. Rev. B* **1988**, *38*, 9797.
(44) Hayashi, S.; Sanda, H.; Agata, M.; Yamamoto, K. *Phys. Rev. B* **1989**, *40*, 5544.
(45) Smith, M. R.; Martell, A. E. *Critical Stability Constants*; Plenum: New York, 1976; Vol. 3, p 163.
(46) Panicker, M. P. R.; Knaster, M.; Kroger, F. A. *J. Electrochem. Soc*. **1978**, *125*, 566.
(47) Sauer, G.; Brehm, G.; Schneider, S.; Nielsch, K.; Wehrspohn, R. B.; Choi, J.; Hofmeister, H.; Gösele, U. *J. Appl. Phys.* **2002**, *91*, 3243.
(48) Li, L.; Li, G. H., Zhang, Y.; Yang, Y. W.; Zhang, L. D. *J. Phys. Chem. B* **2004**, *108*, 19380.
(49) Han, G. C.; Zong, B. Y.; Luo, P.; Wu, Y. H. *J. Appl. Phys.* **2003**, *93*, 9202.
(50) Yoo, W. C.; Lee, J. K. *Adv. Mater.* **2004**, *16*, 1097.